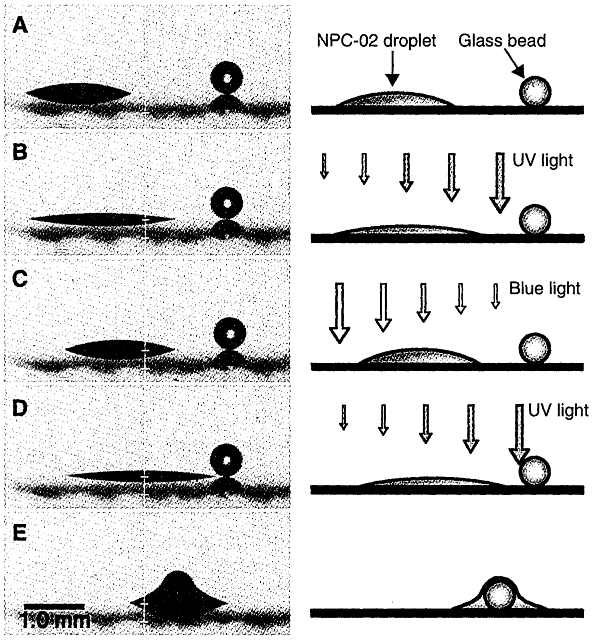

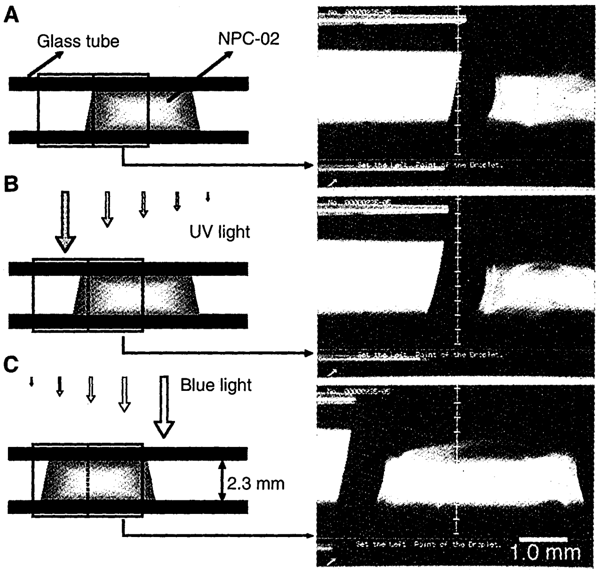

Fig. 5 (left). Light-driven motion of an NPC-02 droplet on a CRA-CM–modified plate to capture a glass bead (diameter ~0.5 mm). A droplet was placed on a CRA-CM–modified plate (**A**), followed by UV light irradiation at the right edge of the droplet to cause an asymmetrical spreading (**B**). Subsequent irradiation with blue light at the left edge resulted in dewetting, leading to the displacement of the droplet (**C**). The repetition of this stepwise photoirradiation resulted in the approach of the droplet to the bead (**D**), which was finally captured by the liquid (**E**). **Fig. 6 (right).** Light-driven displacement of an NPC-02 droplet in a glass tube. A droplet of NPC-02 was placed in the tube (**A**), and one edge of the droplet was exposed to UV light, leading to the slight advancement of the droplet (**B**). Subsequent irradiation with blue light at the opposite edge pushed the droplet to the left (**C**).

taining surfactants can be controlled by light (*26*). In contrast, our work demonstrates a photoinduced liquid motion triggered by azobenzenes immobilized on a solid surface.

15. S.-K. Oh, M. Nakagawa, K. Ichimura, *Chem. Lett.* **4**, 349 (1999).
16. M. Fujimaki *et al.*, *Langmuir* **14**, 4495 (1998).
17. E. Kurita *et al.*, *J. Mater. Chem.* **8**, 397 (1998).
18. Olive oil is a mixture containing fatty acids, vitamins and so on, and contains 55 to 85% oleic acid.
19. Y. L. Chen, C. A. Helm, J. N. Israelachvili, *J. Phys. Chem.* **95**, 10736 (1991).
20. The condition includes both equilibrium thermodynamic and dynamic factors, and is applicable to previously described methods for moving liquids by a driving force arising from an imbalance in surface tension forces. As an example, see (*5*).
21. An NPC-02 drop at 40°C (nematic-isotropic transition temperature of NPC-02 is 35°C) also exhibited the light-driven motion. Detailed studies including the effect of liquid crystallinity on the spreading kinetics of the liquid will be published elsewhere (S.-K. Oh, M. Nakagawa, K. Ichimura, in preparation)..
22. T. Seki, H. Sekizawa, S. Morino, K. Ichimura, *J. Phys. Chem. B* **102**, 5313 (1998).
23. I. Panaiotov, S. Taneva, A. Bois, F. Rondelez, *Macromolecules* **24**, 4250 (1991).
24. F. Brochard, *Langmuir* **5**, 432 (1989).
25. The difference between the advancing and receding dynamic contact angles was less than 2°, even though the advancing and receding edges of the moving droplet would be placed on cis-rich (θ^{cis}_{adv} = 11°) and trans-rich (θ^{tr}_{rec} = 24°) surfaces, respectively.
26. J. Y. Shin and N. L. Abbott, *Langmuir* **15**, 4404 (1999).

21 January 2000; accepted 30 March 2000

Raman Spectroscopy of Iron to 152 Gigapascals: Implications for Earth's Inner Core

Sébastien Merkel,[1,2] Alexander F. Goncharov,[1] Ho-kwang Mao,[1] Philippe Gillet,[2] Russell J. Hemley[1]

Raman spectra of hexagonal close-packed iron (ε-Fe) have been measured from 15 to 152 gigapascals by using diamond-anvil cells with ultrapure synthetic diamond anvils. The results give a Grüneisen parameter γ_0 = 1.68 (±0.20) and q = 0.7 (±0.5). Phenomenological modeling shows that the Raman-active mode can be approximately correlated with an acoustic phonon and thus provides direct information about the high-pressure elastic properties of iron, which have been controversial. In particular, the C_{44} elastic modulus is found to be lower than previous determinations. This leads to changes of about 35% at core pressures for shear wave anisotropies.

Understanding recent geophysical observations of elastic anisotropy, possible superrotation, and magnetism of Earth's inner core (*1*) requires detailed information about the thermodynamic and elastic properties of core-forming materials under appropriate conditions. High-pressure properties of iron are crucial in this respect because the core is composed primarily of this element. Iron transforms from the body-centered cubic (bcc) phase (α-Fe) at ambient conditions to a face-centered cubic (fcc) phase (γ-Fe) at moderate pressures and temperatures and to a higher-pressure hexagonal close-packed (hcp) phase (ε-Fe) (>13 GPa) (*2*). The hcp phase has a wide stability field to more than 300 GPa and high temperatures (*3–5*). Techniques to measure lattice strains at megabar pressures (*6*) have determined the elastic properties of ε-Fe to 210 GPa (*7*). These results show discrepancies with calculations in which first-principles methods were used (*8–10*), in particular for shear moduli and anisotropy. Measurements and estimates of the Grüneisen parameter, an important thermodynamic property of iron that relates the

---

[1] Geophysical Laboratory and Center for High Pressure Research, Carnegie Institution of Washington, 5251 Broad Branch Road, NW, Washington, DC 20015, USA. [2] Laboratoire des Sciences de la Terre, UMR CNRS 5570, Ecole Normale Supérieure de Lyon, 46 allée d'Italie, 69364 Lyon Cedex 07, France.

thermal pressure and the thermal energy, show large discrepancies (*5, 11–16*). Recently, the phonon density of states of ε-Fe at high pressure has been investigated up to 42 GPa (*16*) and 153 GPa (*17*) by inelastic nuclear resonance x-ray scattering. Notable differences with the results of first-principles calculations are also found (*17*). Thus, there is a need to clarify the elastic and thermodynamic properties of iron at core pressures.

Table 1. Thermal Grüneisen γ_0 parameter of ε-Fe and its volume dependence q.

Pressure range (GPa)	γ_0	q	Method
15 to 100	2.2	1	Shock compression (*11*)
15 to 100	2.2 (±0.5)	1.62 (±0.37)	Shock compression (*12*)
20 to 250	2.75	1.5	First-principles (*13*)
0 to 240	1.7	0.7	Theory (*15*)
15 to 300	1.78 (±0.06)	0.69 (±0.10)	X-ray diffraction (*5*)
20 to 42	1.5 (±0.2)	0	Phonon density of states (*16*)
15 to 150	1.68 (±0.20)	0.7 (5)	This study*

*If we fix different values of q, we obtain the following: q = 0, γ_0 = 1.44 (±0.03); q = 1, γ_0 = 1.81 (±0.03); q = 1.5, γ_0 = 2.02 (±0.04).

For many years, it was thought that vibrational Raman spectroscopy of simple metals was not possible at high pressures because of the weak scattering due to the high reflectivity and strong background from the apparatus (e.g., diamond-anvil cell). The bcc (α-Fe) and fcc (γ-Fe) phases have no first-order Raman spectra because all the atoms sit on inversion centers. The ε-Fe hcp phase has one Raman-active mode of E_{2g} symmetry (*18*). Recent studies have shown that the E_{2g} phonon mode in some hcp metals can be measured at moderate pressure in diamond cells. Measurements have been performed on Zn (*19*), Si (*19*), Zr (*20*), and Mg (*21*), but the E_{2g} mode of ε-Fe was expected to be particularly weak (*22*) and has not been reported. Information on the frequency of the E_{2g} mode of ε-Fe and its evolution with pressure provides experimental information on thermodynamic properties of the material because such vibrational frequencies are input data for construction of consistent thermodynamic models (*23*). Moreover, the mode correlates with a transverse acoustic phonon; thus, its frequency shift provides information on the pressure dependence of shear moduli (i.e., C_{44}), which is crucial for constraining the elastic anisotropy of iron at core pressures. Measurement of the phonon also provides a critical test of first-principles methods, which have been a difficult problem for iron.

High-purity polycrystalline Fe samples were loaded in a piston-cylinder–type diamond cell; two sets of experiments were performed at 15 to 50 GPa and 25 to 152 GPa (*24*). To reduce the background luminescence and scattering from the diamond anvils (which could be much stronger than the sample), we used ultrahigh-purity synthetic diamond anvils, which in previous work have been crucial for studying weak Raman excitations in the hundreds of gigapascals pressure range (*25*). We also used a 35° incidence angle for the exciting radiation, which prevents specular reflection from being directed to the spectrometer and reduces the signal from the diamonds. The diameter of the laser spot was less than 10 μm, which is smaller than the sample size, so effects of the pressure gradients are minimized. Signal levels were maximized with a high-throughput single-grating spectrometer with holographic notch filters.

Two Raman bands were observed at moderate pressures (between 15 and 40 GPa), with the stronger band identified as the E_{2g} fundamental predicted by symmetry for the hcp lattice (*26*) (Fig. 1). The mode exhibits a sublinear frequency increase with pressure (Fig. 2). Raman spectra measured together with the ruby fluorescence in different locations of the sample show consistent results. Moreover, spectra measured on compression and decompression are close, which indicates that the uniaxial stress does not have an important effect on these results. The measured frequencies are lower than first-principles results (*27*), although the pressure dependence is similar (Fig. 2). An empirical model (*28*) gives much lower frequencies. The positive pressure shift (initial slope $d\nu_0/dP$ = 1.0 cm^{-1}/GPa) is consistent with the wide stability range of ε-Fe (*3–5*), in contrast to the behavior of several other hcp metals (see below).

We examined the thermal Grüneisen parameter γ_{th} at high pressure. Despite the importance of the Grüneisen parameter of ε-Fe, experimental data have been limited and do not agree (Table 1). The mode-Grüneisen parameter γ_i of the Raman mode is defined as

$$\gamma_i = -[(d\ln\nu)/(d\ln V)] \qquad (1)$$

where ν is the frequency of the mode and V is the volume. It provides an approximate means for calculating γ_{th} with $\gamma_i = \langle\gamma_i\rangle \sim \gamma_{th}$. This assumes that the γ_i for the mode is representative of all the vibrations of the crystal (*23*). We can write

$$\gamma_i \sim \gamma_{th} = \gamma_0(V/V_0)^q \qquad (2)$$

where γ_0 represents the extrapolated value of γ_{th} at zero pressure with the volume dependence of γ_{th} explicitly given by the parameter q. Using this relation and the equation of state of ε-Fe (*3, 29*), we calculate γ_0 = 1.68 (±0.20) and q = 0.7 (±0.5). Assuming q = 1, we have γ_0 = 1.81 (±0.03). The results agree with the analysis of recent high-pressure, high-temperature x-ray diffraction measurements (*5*), which suggests that γ_i of the E_{2g} mode provides a good approximation for $\langle\gamma_i\rangle$. Our analysis is also compatible with that obtained from measurements of the phonon density of state of ε-Fe between 20 and 40 GPa, where q = 0 was assumed (*16*) (Table 1).

In ε-Fe, the C_{44} elastic modulus and the E_{2g} Raman mode are properties of the same phonon branch. Specifically, the E_{2g} mode correlates with a transverse acoustic phonon

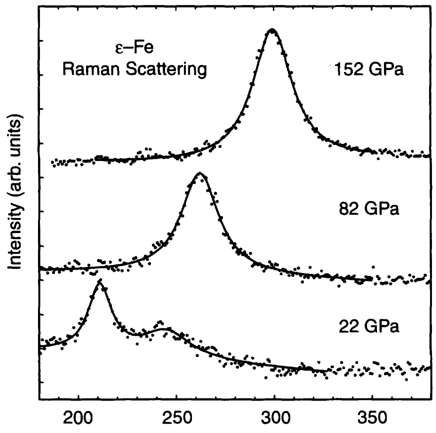

Fig. 1. Raman spectra of ε-Fe at selected pressures. The strong band is identified as the E_{2g} optical phonon; a weaker feature is observed at higher frequencies and lower pressures. Solid line, Lorentzian fit to the peak, which suggests a homogeneous line shape.

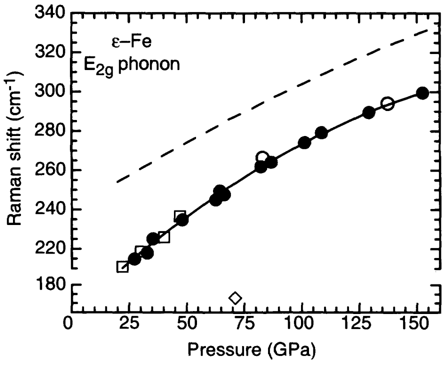

Fig. 2. Pressure shift of E_{2g} Raman phonon in ε-Fe. Open squares, first set of experiments; filled and open circles, second set of experiments during loading and unloading, respectively; solid line, second-order polynomial fit to experimental data; dashed line, fit to the results of first-principles calculations by the techniques described in (*28*) but for ambient temperature (*27*); open diamond, result of an empirical model (*28*).

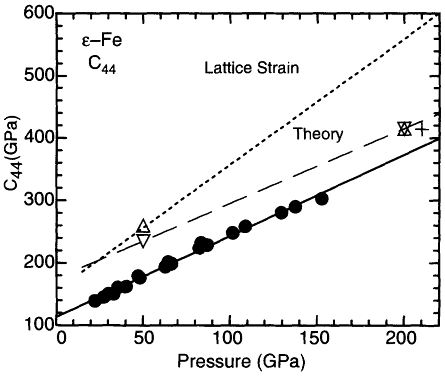

Fig. 3. Pressure dependence of the shear modulus C_{44} of ε-Fe deduced from the E_{2g} phonon frequency. Solid circles, experimental data; solid line, linear fit through the data; up and down triangles, LDA and GGA first-principles calculations, respectively, from (*9*); +, first-principles result (*10*); dashed line, guide to the eye for LDA results; dotted line, pressure dependence determined from lattice-strain measurements (*7*).

and C_{44} represents the slope of this branch at the center of the Brillouin zone. With a phenomenological model, they may be related as

$$C_{44} = 2\pi^2 M[(3)^{1/2}c/(6a^2)]\nu^2 \tag{3}$$

where M is the atomic mass of iron, c and a are unit cell parameters, and ν is the frequency of the optical phonon (*30*). Applying this relation to our data, we deduce the pressure dependence of the C_{44} of ε-Fe (Fig. 3). Notably, our data are lower than the results of lattice-strain experiments (*7*). The analysis used in these experiments assumes that the state of stress on all crystallographic planes is identical. However, recent work has shown that this may not be satisfied in a material undergoing anisotropic deformation, specifically in many hcp transition metals (*31*). The first-principles results (*9*, *10*) are also higher than those obtained here. Application of first principles for magnetic metals such as iron has been problematic, partly because differences between theory and experiments for the pressure-volume relation at low pressures (*32*) may be associated with changes of the magnetic properties within ε-Fe (*9*). The use of Raman spectroscopy to determine the pressure dependence of C_{44} is exact for a sine dispersion relation; if the phonon branch does not deform with pressure, this assumption can be supported by theory (*27*, *28*).

Table 2. Raman shift and deduced and measured C_{44} elastic modulus at zero pressure for three hcp metals.

Element	Raman shift (cm^{-1})	C_{44} (GPa)	
		Calc.	Exp.
Zr	87 (*20*)	28.9	33.4 (*37*)
Mg	122 (*21*)	15.9	18.6 (*37*)
Zn	71.5 (*19*)	19.8	39.6 (*37*)

The results have important geophysical implications. Although knowledge of C_{44} is not sufficient to calculate the full seismic anisotropy parameters, the shear wave polarized perpendicular to the basal plane (S1) and that polarized parallel to the basal plane (S2) have the anisotropies

$$\Delta_{S1} = (C_{11}+C_{33}-2C_{13})/4C_{44},\quad \Delta_{S2} = C_{44}/C_{66} \tag{4}$$

Therefore, the lower value of C_{44} found here would increase Δ_{S1} and decrease Δ_{S2}. Assuming no difference in the estimation of the other elastic moduli (*7*) arising from the change of C_{44}, we calculate $\Delta_{S1} \approx 0.65$ and $\Delta_{S2} \approx 1.44$ at 39 GPa, corresponding to changes of about 35%. This also improves the agreement with the first-principles calculations (*33*).

Finally, we can compare the results with those of other hcp structured transitions metals that have been studied recently by high-pressure Raman spectroscopy—for example, Zn (*19*), Si (*19*), Zr (*20*), and Mg (*21*). The behavior of the E_{2g} phonon with pressure differs appreciably from one to another. Zn, Si, and Mg show an increase of frequency with pressure with initial slopes ($d\nu_0/dP$) of about 3.3, 3.1, and 3 cm^{-1}/GPa, respectively. In contrast, ε-Fe also shows a positive pressure shift but with a $d\nu_0/dP$ of 1.0 cm^{-1}/GPa. Comparing γ_i values, we find γ_i(Zn) ≈ 2.4 between ambient pressure and 12 GPa, γ_i(Mg) ≈ 1.6 at ambient pressure, and γ_i(Si) ≈ 6 near 40 GPa compared with γ_i(Fe) = 1.44 (±0.03) between 20 and 150 GPa. Zirconium appears to be a unique case: mode softening is observed for the E_{2g} phonon of α-Zr, with $d\nu_0/dP = -0.7$ cm^{-1}/GPa (*20*). Moreover, the relation between elastic modulus C_{44} and the frequency of the E_{2g} mode (Eq. 3) can be examined for Zr, Mg, and Zn because they crystallize in the hcp structure at zero pressure and reliable experimental measurements of C_{44} are available (Table 2). The results agree to within 15% for Zr and Mg, but a large discrepancy is found for Zn, which undergoes higher-pressure phase transition and anomalous changes in electronic structure (*34*) (not evident in Fe). Direct comparison of the measured and calculated frequency of the E_{2g} phonon at different pressures is possible for Mg (*35*) and Zr (*36*). In both cases, we find that the measured frequency is lower than that calculated by first-principles methods, which is consistent with results obtained for ε-Fe (Figs. 2 and 3). This study and analysis open the possibility of Raman investigations of the vibrational dynamics of other metals, including planetary core-forming materials at megabar to multimegabar pressures.

References and Notes

1. X. Song and P. G. Richards, *Nature* **382**, 221 (1996); W. Su, A. M. Dziewonski, R. Jeanloz, *Science* **274**, 1883 (1996); G. A. Glatzmaier and P. H. Roberts, *Science* **274**, 1887 (1996); W. Kuang and J. Bloxham, *Nature* **389**, 371 (1997).
2. T. Takahashi and W. A. Bassett, *Science* **145**, 483 (1964); F. P. Bundy, *J. Appl. Phys.* **36**, 616 (1965); J. M. Brown and R. G. McQueen, *J. Geophys. Res.* **91**, 7485 (1986); R. Boehler, N. von Bargen, A. Chopelas, *J. Geophys. Res.* **95**, 21731 (1990).
3. H. K. Mao, Y. Wu, L. C. Chen, J. F. Shu, A. P. Jephcoat, *J. Geophys. Res.* **95**, 21737 (1990).
4. G. Shen, H. K. Mao, R. J. Hemley, T. S. Duffy, M. L. Rivers, *Geophys. Res. Lett.* **25**, 373 (1998); G. Shen and D. L. Heinz, *Rev. Mineral.* **37**, 369 (1998). These studies have shown that the fcc-hcp liquid-triple point is at 60 GPa and 2500 K, with the hcp phase stable at higher pressures and temperatures (at least 155 GPa and 3000 K). The stability of ε-Fe at core conditions is also consistent with recent shock-wave results [J. H. Nguyen and N. C. Holmes, personal communication] as well as theory [L. Vočadlo, J. Brodholt, D. Alfè, M. J. Gillan, G. D. Price, *Phys. Earth Planet. Inter.* **117**, 123 (2000)].
5. L. S. Dubrovinsky, S. K. Saxena, N. A. Dubrovinskaia, S. Rekhi, T. Le Bihan, *Am. Mineral.* **85**, 386 (2000); L. S. Dubrovinsky, S. K. Saxena, F. Tutti, S. Rekhi, T. Le Bihan, *Phys. Rev. Lett.* **84**, 1720 (2000). These studies indicate that the hcp phase is stable to at least 300 GPa and 1500 K.
6. R. J. Hemley *et al.*, *Science* **276**, 1242 (1997); A. K. Singh, H. K Mao, J. Shu, R. J. Hemley, *Phys. Rev. Lett.* **80**, 2157 (1998); A. K. Singh, C. Balasingh, H. K Mao, R. J. Hemley, J. Shu, *J. Appl. Phys.* **83**, 7567(1998).
7. H. K. Mao *et al.*, *Nature* **396**, 741 (1998) [correction, *Nature* **399**, 280 (1999)].
8. L. Stixrude and R. E. Cohen, *Science* **267**, 1972 (1995).
9. G. Steinle-Neumann, L. Stixrude, R. E. Cohen, *Phys. Rev. B* **60**, 791 (1999).
10. A. Laio, S. Bernard, G. L. Chiarotti, S. Scandolo, E. Tosatti, *Science* **287**, 1027 (2000).
11. R. G. McQueen *et al.*, in *High Velocity Impact Phenomena*, R. Kinslow, Ed. (Academic Press, San Diego, CA, 1970), p. 296.
12. R. Jeanloz, *J. Geophys. Res.* **84**, 6059 (1979).
13. E. Wasserman, L. Stixrude, R. E. Cohen, *Phys. Rev. B* **53**, 8296 (1996).
14. L. Stixrude, E. Wasserman, R. E. Cohen, *J. Geophys. Res.* **102**, 24729 (1997).
15. O. L. Anderson, *Phys. Earth Planet. Inter.* **109**, 179 (1998).
16. R. Lübbers, H. F. Grünsteudel, A. I. Chumakov, G. Wortmann, *Science* **287**, 1250 (2000).
17. H.-K. Mao *et al.*, unpublished data.
18. The hcp structure has two atoms per unit cell, which are located on sites of symmetry D_{3h}. The six normal modes of zero wave vector belong to the irreducible representations $A_{2u} + B_{1g} + E_{1u} + E_{2g}$. The B_{1g} and E_{2g} are optical phonons polarized along and perpendicular to the optical axis, respectively. The doubly degenerate E_{2g} mode is Raman active.
19. H. Olijnyk, *High Pressure Res.* **10**, 461 (1992); H. Olijnyk, *Phys. Rev. Lett.* **68**, 2232 (1992).
20. H. Olijnyk and A. P. Jephcoat, *Phys. Rev. B* **56**, 10751 (1997).
21. H. Olijnyk and A. P. Jephcoat, in *Program of the AIRAPT-XVII Conference*, M. H. Manghnani, Ed. [*International Association for the Advancement of High Pressure Science and Technology* (AIRAPT), Honolulu, HI, 1999], p. 148.
22. A. P Jephcoat, H. Olijnyk, K. Refson, *Eos* **80**, F929 (1999).
23. P. Gillet, R. J. Hemley, P. F. McMillan, *Rev. Mineral.* **37**, 525 (1998).
24. The gasket material was W for the first experiment and Rh for the second experiment. There was no pressure medium. Raman spectra were excited with the 488- and 514.5-nm lines of an argon-ion laser and measured with a single-grating ISA HR-460 spectrometer equipped with a charged-coupled device (CCD) detector. Pressures were determined by the ruby fluorescence method [H. K. Mao, J. Xu, P. M. Bell, *J. Geophys. Res.* **91**, 4673 (1986)].
25. A. F. Goncharov, R. J. Hemley, H. K. Mao, J. Shu, *Phys. Rev. Lett.* **80**, 101 (1998); A. F. Goncharov, V. Struzhkin, H. K. Mao, R. J. Hemley, *Phys. Rev. Lett.* **83**, 1998 (1999).
26. The low-frequency band becomes stronger with pres-

sure, which suggests increased ordering of the hcp lattice and that the high-frequency weak band is disorder induced. The high-frequency band remained in the spectra on pressure release to 7 GPa, unlike the hcp Raman phonon, which disappears at the phase transition back to bcc α-Fe.
27. L. Vočadlo, personal communication.
28. D. Alfèe, G. D. Price, M. J. Gillan, *Phys. Rev. B*, in press.
29. A. P. Jephcoat, H. K. Mao, P. M. Bell, *J. Geophys. Res.* **91**, 4677 (1986).
30. This relation can be derived with a three-body force model for an hcp solid with a nonideal *c*/*a* ratio [J. C. Upadhyaya, D. K. Sharma, D. Prakash, S. C. Upadhyaya, *Can. J. Phys.* **72**, 61(1994)].
31. H. R. Wenk, S. Matthies, J. Shu, R. J. Hemley, H.-K. Mao, *Nature*, submitted; see also [H. R. Wenk, T. Takeshita, R. Jeanloz, G. C. Johnson, *Geophys. Res. Lett.* **15**, 76 (1988)].
32. L. Stixrude, R. E. Cohen, D. J. Singh, *Phys. Rev. B* **50**, 6442 (1994).
33. For example, at a reference pressure of 210 GPa [see (*10*)], the lattice-strains experiments (*7*) lead to Δ_{S1} = 0.60 and Δ_{S2} = 1.70, the first-principles LDA calculations (*9*) give Δ_{S1} = 1.27 and Δ_{S2} = 0.99, and the first-principles OP calculations (*10*) give Δ_{S1} = 1.03 and Δ_{S2} = 1.02. If we extrapolate the C_{44} calculated here and substitute it into the lattice-strains results (*7*), we deduce Δ_{S1} = 0.91 and Δ_{S2} = 1.12, which is closer to theory.
34. K. Takemura, in *Program of the AIRAPT-XVII Conference*, M. H. Manghnani, Ed. (AIRAPT, Honolulu, HI, 1999), p. 150.
35. J. D. Althoff, P. B. Allen, R. M. Wentzcovitch, *Phys. Rev. B* **48**, 13253 (1993).
36. S. A. Ostanin, E. I. Salamatov, V.Y. Trubitsin, *Phys. Rev. B* **58**, 15962 (1998).
37. E. A. Brandes, Ed. *Smithells Metals Reference Book* (Butterworths, London, 1983); F. Marinelli, M. Roche, I. Baraille, C. Pauchan, *Phys. Rev. B* **54**, 6054 (1996).

38. We thank L. Vočadlo for communicating unpublished results and very helpful correspondence; we are grateful to V. V. Struzhkin, E. Gregoryanz, and R. E. Cohen for useful discussions and P. McMillan and other reviewers for their comments.

13 March 2000; accepted 19 April 2000

Accretion of Primitive Planetesimals: Hf-W Isotopic Evidence from Enstatite Chondrites

Der-Chuen Lee[1,2] and Alex N. Halliday[2]

Enstatite chondrites have often been considered to be closely related to the material from which Earth accreted. However, tungsten isotopic data reveal clear differences. Moreover, the silicate and metal fractions define distinct initial ^{182}Hf/^{180}Hf corresponding to a 13.8 ± 5.3 million year apparent age difference. Internal reequilibration does not provide a ready explanation for this result. Larger scale redistribution of tungsten is more likely, such as may have occurred during collisions between planetesimals.

Enstatite chondrites formed in a highly reduced environment, possibly in the inner regions of the solar nebula (*1*, *2*). They are the only group of chondrites whose silicate fractions have oxygen isotopic compositions similar to those of Earth and the moon (*3*), prompting some to suggest a genetic relationship (*4*). The Mn-Cr isotopic data for enstatite chondrite leachates and residues define an initial Cr isotopic composition that is similar to that of silicate Earth and the moon (*5*, *6*), and this has been used to argue that the enstatite chondrite parent body (ECPB) may have formed at the same heliocentric distance. However, many features of enstatite chondrites are enigmatic and hard to explain. There are substantial compositional gaps between the enstatite chondrites and the Earth-moon system (*2*, *7*), and chemical evidence for heterogeneous accretion of the ECPB has been presented (*8*). Furthermore, the relationship with Earth is unlikely to be straightforward. For example, dynamic simulations suggest that localized feeding zones for the growth of planetesimals and planets are unrealistic (*9*). Rather, planetary accretion can sample a broad provenance (*9*, *10*).

The recently developed ^{182}Hf-^{182}W chronometer (half-life = 9 million years) is well suited for studying accretion in the inner solar system (*11*–*15*). Both Hf and W are highly refractory. However, chemically they are quite different, with Hf being strongly lithophile ("silicate-loving") and W moderately siderophile ("metal-loving"), such that fractionation between Hf and W occurs during metal-silicate differentiation and partial melting (*11*, *12*). Hence, excess ^{182}W in the W atomic abundance is found in meteorites that sample high Hf/W silicate reservoirs formed within the life-span of ^{182}Hf. This is as found in some eucrites, martian meteorites, lunar samples, and the silicate phases of ordinary chondrites (*13*–*15*). Conversely, a deficit in ^{182}W is found in early metals such as iron meteorites and the metal fractions of ordinary chondrites, because they have low Hf/W (*10*, *11*, *16*, *17*). Ordinary chondrites appear to define reasonable internal Hf-W isochrons with a linear functional relation between Hf/W and W isotopic compositions. Here we report data for enstatite chondrites and find different behavior implying systematic redistribution and mixing of W.

Four enstatite chondrites, including EH and EL groups, Abee (EH4), Indarch (EH4), ALHA81021 (EL6), and Hvittis (EL6), were selected for study. Experimental procedures (*18*) were as used previously (*15*). The Hf-W data for all four enstatite chondrites (Table 1) show a positive correlation between measured Hf/W ratios and the respective W isotopic compositions of individual fractions (Fig. 1), consistent with the former presence of ^{182}Hf. In detail, however, the metals and silicates display distinct characteristics (Fig. 1).

Portions of the magnetic (largely metal) fractions of each meteorite were leached in 6 M HCl (*18*). The leachates contain the easily soluble metal, sulfide, and minor phosphate fractions with low Hf/W (Table 1). The residues from this procedure mainly comprise small amounts of silicates and minor oxides, insoluble in 6 M HCl. The Hf-W data for all of these "magnetic fractions," that is, bulk metals, metal leachates, and metal residues, are collinear, intersecting the data for the carbonaceous chondrites, Allende and Murchison (*11*, *12*) (Fig. 1). These data are also collinear with the data for the ordinary chondrites (*15*), providing evidence that the metals are coeval and early (Web fig. 1) (*19*). A regression of the data for all enstatite chondrite metals, their leachates and residues, and the whole rock values of Allende and Murchison yields a slope (equal to initial ^{182}Hf/^{180}Hf) of $(1.85 \pm 0.38) \times 10^{-4}$ (Fig. 2), equivalent to that defined by the ordinary chondrites ($\sim 1.8 \times 10^{-4}$) (*15*). The regression results are the same but with larger uncertainties if the carbonaceous chondrites are excluded [$(1.88 \pm 0.73) \times 10^{-4}$]. The initial ^{182}Hf/^{180}Hf at the start of the solar system is thought to lie in the range $(1.87 \pm 0.16) \times 10^{-4}$ to $(2.75 \pm 0.24) \times 10^{-4}$ (*15*). On this basis, the metals in the enstatite chondrites formed within a few million years, at most, of the start of the solar system.

In contrast, the nonmagnetic fractions (predominantly silicates) for each sample lie to the right of and below the best-fit line defined by the magnetic (metal) fractions (Fig. 1). The data for the nonmagnetic frac-

---

[1]Department of Geological Sciences, University of Michigan, Ann Arbor, MI 48109-1063, USA. [2]Institute for Isotope Geology and Mineral Resources, Department of Earth Sciences, ETH Zürich, CH-8092, Zürich, Switzerland.